

Gating by Tryptophan 73 Exposes a Cryptic Pocket at the Protein-Binding Interface of the Oncogenic eIF4E Protein

Dilraj Lama,^{*,†} Christopher J. Brown,[‡] David P. Lane,[‡] and Chandra S. Verma^{*,†,§,||}

[†]Bioinformatics Institute, A*STAR (Agency for Science, Technology and Research), 30 Biopolis Street, #07-01 Matrix, Singapore 138671

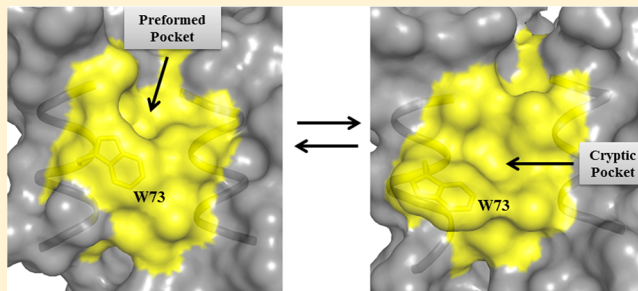
[‡]p53 Laboratory, A*STAR (Agency for Science, Technology and Research), 8A Biomedical Grove, #06-04/05, Neuros/Immunos, Singapore 138648

[§]Department of Biological Sciences, National University of Singapore, 14 Science Drive 4, Singapore 117543

^{||}School of Biological Sciences, Nanyang Technological University, 50 Nanyang Drive, Singapore 637551

Supporting Information

ABSTRACT: Targeting protein–protein interacting sites for potential therapeutic applications is a challenge in the development of inhibitors, and this becomes more difficult when these interfaces are relatively planar, as in the eukaryotic translation initiation factor 4E (eIF4E) protein. eIF4E is an oncogene that is overexpressed in numerous forms of cancer, making it a prime target as a therapeutic molecule. We report here the presence of a cryptic pocket at the protein-binding interface of eIF4E, which opens transiently during molecular dynamics simulations of the protein in solvent water and is observed to be stable when solvent water is mixed with benzene molecules. This pocket can also be seen in the ensemble of structures available from the solution-state conformations of eIF4E. The accessibility of the pocket is gated by the side-chain transitions of an evolutionarily conserved tryptophan residue. It is found to be feasible for accommodating clusters of benzene molecules, which signify the plasticity and ligandability of the pocket. We also observe that the newly formed cavity provides a favorable binding environment for interaction of a well-recognized small molecule inhibitor of eIF4E. The occurrence of this transiently accessible cavity highlights the existence of a more pronounced binding groove in a region that has traditionally been considered to be planar. Together, the data suggest that an alternate binding cavity exists on eIF4E and could be exploited for the rational design and development of a new class of lead compounds against the protein.



The eukaryotic initiation factor 4E (eIF4E) protein recognizes mRNA molecules during the initial stages of translation and has a critical role in mediating cap-dependent translation.^{1,2} Overexpression of this molecule is associated with many different forms of cancer^{3–5} and as such is a prime target as an anticancer therapeutic molecule.^{6,7} Small molecules, oligonucleotides, and peptide-based inhibitors are currently being designed to develop potential drugs against eIF4E.^{8–13} There are two regions on the surface of eIF4E that are exploited for structure-based design of inhibitors against the protein. These are the “cap-binding” and “protein-binding” sites (Figure 1). The cap-binding site identifies the 7-methylguanosine-containing cap present at the 5' end of mRNA,¹⁴ and the protein-binding interface interacts with the eIF4G protein¹⁵ during the formation of translation initiation complex eIF4F. This assembly is subsequently delivered to the ribosomal complex to form the macromolecular machinery required to scan for the start codon on the mRNA and initiate translation.^{1,2} The interaction between eIF4E and eIF4G is modulated by other proteins such as 4E-BP that also bind to the same protein-binding interface.¹⁶ Experimentally determined structures of eIF4E in complex

with peptide fragments derived from eIF4G1 and 4E-BP1 proteins have clearly demonstrated that both molecules have very similar modes of interaction (Figure 1).^{14,15} This has guided the development of potent peptide inhibitors against eIF4E.^{9,12,17} However, this interface is relatively planar, which makes it quite exceptional compared to, for example, the interfaces of the MdM2:p53 system and the Bcl-2 protein family that have pronounced hydrophobic binding grooves.^{18–20} Thus it is very challenging to design molecules that would competitively target this location in eIF4E to disrupt the interactions with its binding partners. The cap-binding site on the other hand is concave and is reported to bind a small molecule “ribavirin” that is proposed to act as an antagonist against eIF4E.^{21,22} Other structure-guided drug design efforts have led to the development of promising lead inhibitors targeting this binding interface.¹¹

Received: July 21, 2015

Revised: September 29, 2015

Published: October 2, 2015



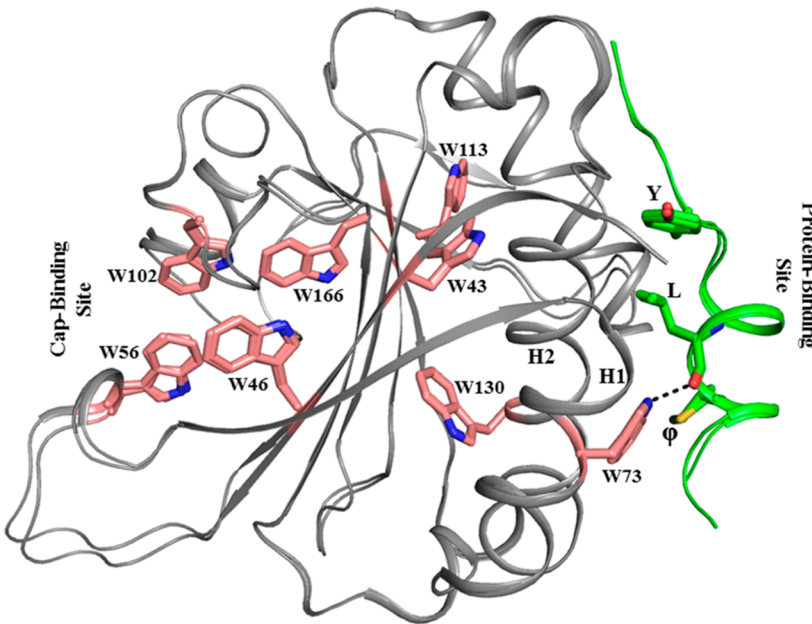


Figure 1. Superimposition of crystal structures of eIF4E in complex with eIF4G1 and 4E-BP1 peptides. The structures are PDB entries 2W97 and 2V8W, respectively. The evolutionarily conserved tryptophan residues in eIF4E and the “YXXXXL Φ ” motif present in eIF4G1 and 4E-BP1 are shown. Cap- and protein-binding sites are present on opposite sides of the molecule. The conserved hydrogen bond between the side-chain of W73 from eIF4E and the backbone of the leucine residue from eIF4G1/4E-BP1 is indicated.

Table 1. Side-Chain χ^2 Torsion Angles of W73 in Experimental Structures^a

	PDB entry	method ^b	structural states	organism	χ^2 (deg) ^c	ref
1	2V8W	X-ray 2.3 Å	eIF4E:4E-BP1:m ⁷ GTP	human	117.2	14
2	2W97, A ^d	X-ray 2.3 Å	eIF4E:eIF4G1:m ⁷ GTP	human	113.5	15
3	3TF2	X-ray 2.1 Å	eIF4E	human	106.3	28
4	1L8B	X-ray 1.8 Å	eIF4E:m ⁷ GTP	mouse	112.4	53
5	1EJ1	X-ray 2.2 Å	eIF4E:m ⁷ GDP	mouse	110.2	25
6	2IDV	X-ray 2.3 Å	eIF4E:m ⁷ GDP	wheat	116.7	52
7	2IDR	X-ray 1.9 Å	eIF4E	wheat	112.4	52
8	2WMC	X-ray 2.2 Å	eIF4E:m ⁷ GTP	pea	108.2	51
9	2GPQ	NMR (10 models)	eIF4E	human	-54.6 to 128.4	56
10	1RF8	NMR (11 models)	eIF4E:eIF4G1:m ⁷ GDP	yeast	127.9–144.2	54
11	1AP8	NMR (20 models)	eIF4E:m ⁷ GDP	yeast	-0.5 to -74.4	55

^aRepresentative eIF4E structures in apo, binary, and ternary structural states were obtained from the PDB. m⁷GTP (7-methylguanosine triphosphate) and m⁷GDP (7-methylguanosine diphosphate) are mRNA cap analogues. ^bIf the structure is determined by X-ray, the resolution of the structure is shown, and for structures determined by NMR, the number of models present in the structure is given in parentheses. ^cThe χ^2 side-chain torsion angle was measured along heavy atoms CA, CB, CG, and CD2 of W73. For the NMR structures, the angle was measured for all the available models and the range as obtained is shown. ^dFor 2W97, only chain A was considered.

eIF4E proteins from different organisms possess eight conserved tryptophan residues that have distinct structural and functional roles (Figure 1).²³ W56, W102, and W166 are involved in the recognition of the cap structure, while W43, W46, W113, and W130 are part of the hydrophobic core that is probably responsible for maintaining the structural stability of the protein. Conserved W73 is present at the site of recognition between eIF4E and eIF4G1/4E-BP1 proteins. Both proteins share the common recognition motif “YXXXXL Φ ” (Φ signifies any hydrophobic residue) that is critical for their interactions with eIF4E.²⁴ In this interaction, the side-chain of W73 is involved in the formation of a hydrogen bond with the backbone of the strictly conserved leucine of eIF4G1 and 4E-BP1 (Figure 1). This traditional mode of interaction between eIF4E and its binding partners is well-established.^{14,15,24,25} However, there are also reports of proteins that interact with eIF4E without utilizing

the common binding motif and may interact at the same interface, but in a different binding mode.^{26,27} These suggest that the protein-binding interface of eIF4E could potentially be highly plastic and exhibit alternate binding modes with different molecules.

In this work, we report the discovery of a cryptic binding pocket in the protein-binding site of eIF4E that is regulated by the conformational flexibility of W73 and the plasticity of the interface region. The pocket is visible in some of the structures determined by NMR spectroscopy. Molecular dynamics (MD) simulations of the apo and holo forms of the protein suggest that W73 accesses different orientations, resulting in the transient exposure of a hydrophobic pocket on the protein-binding interface. In a benzene saturation simulation, this cavity showed the potential to accommodate multiple benzene molecules. It also provides a more favorable environment for the binding of a

small molecule that is known to interact with eIF4E. These observations indicate the identification of a novel binding pocket on eIF4E that could be exploited for future designs of inhibitors against the oncogenic protein.

MATERIALS AND METHODS

Initial Structures. The crystal structures of eIF4E in the apo-state (PDB entry 3TF2)²⁸ and in complex with the eIF4G1 peptide and m⁷GTP (7-methylguanosine triphosphate) cap analogue (PDB entry 2W97)¹⁵ were downloaded from the Protein Data Bank (Table 1). The peptide and the cap from 2W97 were manually removed to generate an alternate uncomplexed structure of eIF4E that we term the “holo” structure. Both the apo and holo structures represented the two separate starting states for the different uncomplexed simulations of eIF4E. The effective length of eIF4E considered for the study is K36–V217 (residue numbering according to Uniprot entry P06730). The N-terminus of the protein was capped using ACE (acetylate), while the C-terminus was capped with NME (N-methylamide). These structures were placed in a cuboid box with TIP3P water²⁹ such that the minimal distance from the edge of the box was 12 Å (dimensions of 75.5 Å × 73.3 Å × 77.1 Å). The net charge of the system was +3, which was accordingly neutralized by adding three chloride ions using the TLEAP module of AMBER12.³⁰

Molecular Dynamics Simulations. Molecular dynamics (MD) simulations were performed in AMBER12³⁰ using the PMEMD module and employing the all-atom ff99SB force field.³¹ The solvated systems were energy minimized using the steepest descent and conjugate gradient algorithms, then gradually heated to a temperature of 300 K, and subsequently equilibrated for a period of 500 ps. Each system was then subjected to the production phase of MD simulations. The NVT (constant number, volume, and temperature) ensemble was used during the heating phase, and NPT (constant number, pressure, and temperature) conditions were used during the equilibration and production phases. Langevin dynamics^{32,33} with a collision frequency of 1.0 ps⁻¹ were used for temperature regulation, and a weak coupling³⁴ with a relaxation time of 1 ps was employed to maintain the pressure at 1 atm. The periodic boundary condition was appropriately applied, and the particle mesh Ewald (PME) method³⁵ was used for calculating long-range electrostatic interactions. All bonds involving hydrogen atoms were constrained using the SHAKE algorithm³⁶ with an integration time step of 2 fs.

Mixed-Solvent Molecular Dynamics Simulations. The energy-minimized apo and holo structures were used as starting structures for mixed-solvent simulations that were conducted using a mixture of water and benzene molecules. Such cosolvent simulation approaches have previously been shown to improve the sampling as compared to pure water simulations and hence assist in identifying conformations of proteins that are more significant for ligand binding.^{37–41} In particular, the benzene saturation simulations used in this work have been rigorously benchmarked by Tan et al.³⁹ to demonstrate the general applicability of this method for the identification of potential binding pockets on protein surfaces. The program Packmol⁴² was used to generate different initial structures of the protein and benzene system that differed in the placement of an appropriate number of benzene molecules [depending on the molarity (Table 2)] within 35 Å of the protein center. These systems were then neutralized with three chloride ions and solvated with TIP3P water molecules in a cuboid box with dimensions of 75.5

Table 2. Frequency of Occurrence of the Open State Conformation of W73 in Mixed-Solvent Simulations^a

	0.0 M	0.1 M	0.2 M	0.3 M	0.4 M
no. of benzenes	0	30	60	90	120
apo	10%	30%	30%	40%	40%
holo	10%	20%	30%	40%	50%

^aTwo different starting states (apo and holo) of eIF4E were used. Ten independent MD simulation replicates were conducted for each system at different molar concentrations of benzene. The conformational transition of W73 was measured with the χ^2 side-chain torsion angle, and the system was defined to access the open state if the residue underwent transition at least once (see Figure S3) during the simulation period.

Å × 73.3 Å × 77.1 Å, which was the same as that used previously for the apo/holo eIF4E simulations in pure water solvent to maintain a constant volume (Figure S1). Minimization, equilibration, and production MD simulations were conducted as described above. RESP (restrained electrostatic potential) atomic charges for benzene were derived using the project W-46 from the R.E.D. server database.⁴³ The atom type definition and the associated force field parameters were obtained from the GAFF force field⁴⁴ using Antechamber in AMBER12.³⁰

Benzene and Water Occupancy Map. Occupancy maps of benzene and water were generated by using the grid command in the PTTRAJ module of AMBER12.³⁰ The calculations were conducted on the simulated trajectories with grid cells of size 0.5 Å × 0.5 Å × 0.5 Å, and the number of molecules of interest (benzene or water) within each grid cell was counted. The raw data generated from this calculation were analyzed using the volume viewer in the Chimera visualization software.⁴⁵ The cutoff isovalue for benzene is adjusted such that we observe no benzene clusters in the bulk. For water, the cutoff was set to 2.5 times the peak value, which is the mode of the isovalue distribution. These are arbitrary criteria that allow the removal of weak binding sites and preserve locations that can be classified as bound waters or benzene.

Docking and Simulation of 4E1RCat. The three-dimensional coordinates of the small molecule 4E1RCat was downloaded from PubChem (entry 16195554). The conformations of eIF4E in the closed and open state were selected from MD-simulated structures as representatives from the largest population in the respective clusters. The small molecule was docked against eIF4E with a flexible ligand and rigid macromolecule using AutoDock version 4.2 through the AutoDock-Tools graphical user interface.⁴⁶ A search space of 60 Å × 60 Å × 60 Å was used centered in the vicinity of the residues forming the cryptic pocket. Docking was performed using the Lamarckian genetic algorithm with an initial population size of 150 random states of the small molecule that would be docked in the defined space of the protein with 25000000 energy evaluations for each run. We selected the 20 lowest-energy poses for both the closed and open states as the final set of docked conformations for comparative analysis. The docked poses were then clustered on the basis of the binding energy as computed by Autodock. One representative structure from the first three lowest-energy clusters was chosen to perform MD simulation of 200 ns each following the same protocol and parameters as described above. The RESP-based atomic charges for the small molecule ligand were obtained through the RED server⁴⁷ using the RESP-A1A (HF-6-31G*) charge model and the Gaussian_2009_C.01 quantum mechanics program. The other force field parameters

were derived using the GAFF force field⁴⁴ through Antechamber in AMBER12.³⁰

MM/GBSA Binding Energy Calculation. An estimate of the binding energy was calculated with the MM/GBSA (molecular mechanics/generalized Born surface area)⁴⁸ method using the MMPBSA.py script.⁴⁹ One thousand structures covering the simulation period were extracted at equal intervals, and the generalized Born solvation model⁵⁰ was used for the implicit representation of the solvent molecules, with a salt concentration of 0.15 mM. The solvent accessible surface area was computed using a recursive method of approximating a sphere around an atom starting from an icosahedral shape.

RESULTS

Evolutionarily Conserved W73 Adopts Multiple Conformational States. W73 is one of the eight evolutionarily conserved tryptophan residues in eIF4E proteins (Figure 1).²³ It facilitates the specificity of interactions between eIF4G1/4E-BP1 peptide fragments and eIF4E through the formation of a conserved hydrogen bond between its side-chain nitrogen and the backbone oxygen of the strictly conserved leucine residue in the peptides. W73 is observed to have a specific orientation in these structures (PDB entries 2V8W and 2W97)^{14,15} as indicated here with the side-chain χ^2 (measured along CA, CB, CG, and CD2) dihedral for the residue (Table 1). Analysis of other crystal structures of eIF4E (PDB entries 3TF2, 1L8B, 1EJ1, 2IDV, 2IDR, and 2WMC),^{25,28,51–53} where the protein is not in complex with interacting peptides, shows that the residue has an orientation similar to that observed in the complexes with the χ^2 torsion angle ranging from $\sim 106^\circ$ to 117° . The conformational states of the residue in these structures are shown in Figure 2A. Interestingly, in the solution-state structures of this protein (PDB entries 2GPQ, 1RF8, and 1AP8),^{54–56} the residue adopts multiple orientations as can be seen from the dihedral angle values of the different models in these structures (Table 1). In 1RF8, eIF4E is in complex with the eIF4G1 peptide. The residue however adopts a slightly different conformation as compared to the crystal structures mentioned above with an average χ^2 of $\sim 135^\circ$. In 1AP8, where the protein is not in complex with the peptide, χ^2 values for all the models vary between -0.5° and -74° . This not only is distinctly different from that seen in the crystal structures but also spans a very wide range. In the solution-state apo structure of eIF4E (PDB entry 2GPQ), consisting of the 10 lowest-energy structures, χ^2 adopts a range of conformations, including those seen in the crystal structures, covering a range from approximately -54° to 128° . Superimposition of representative model structures of eIF4E derived from NMR with the X-ray structures shows the different possible orientations that W73 can adopt (Figure 2A).

Explicit solvent MD simulations of eIF4E initiated from two different starting structures (PDB entry 3TF2 for the apo form and PDB entry 2W97 for the holo form) showed the presence of three major conformational states of W73 in the generated ensemble of structures (Figure 2B, top) (movie S1). The range of χ^2 values for the different states are $90\text{--}180^\circ$, $30^\circ\text{--}60^\circ$, and $-60^\circ\text{--}150^\circ$. The most populated state from 90° to 180° includes conformational states represented by the X-ray structures, whereas the other two less populated states include conformations of the residues seen in the NMR structures. Although the MD simulations were started with the X-ray conformers, it is clear that during the simulations, the residue interconverts among the various conformational states (Figure

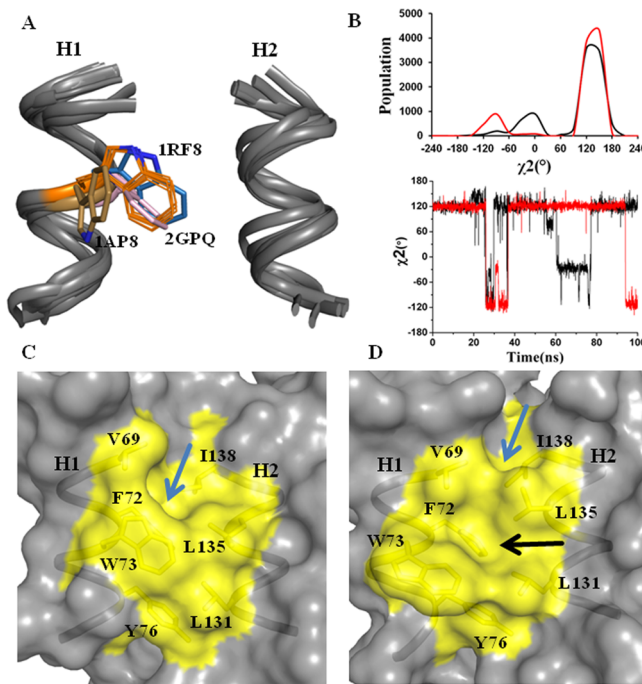


Figure 2. Different conformational states of W73 observed in experimental and simulated structures. (A) Superimposition of experimentally determined structures of eIF4E (see Table 1 for details) depicting the different conformational states of W73 as observed in X-ray and representative lowest-energy structures from three NMR structures (PDB entries 2GPQ, 1RF8, and 1AP8); the helices shown are H1 and H2. (B, top) Population distribution of W73 in terms of its χ^2 side-chain torsion angle in MD simulations of the unbound state of eIF4E (black for apo and red for holo). (B, bottom) Time series plot of the χ^2 side-chain dihedral angle of W73 in the same simulations. (C) Protein-binding interface of eIF4E comprising of helices H1 and H2 shown with W73 in the closed state (PDB entry 3TF2) and (D) open state conformations (snapshot from the 3TF2 simulation). The hydrophobic residues lining this region are represented and colored yellow. The blue arrow points to the preformed pocket, and the black arrow indicates the cryptic pocket created after the transition of W73.

2B, bottom) that are observed in the X-ray and NMR structures (Table 1).

Exposure of a Cryptic Pocket at the Protein-Binding Interface. W73 is located in the protein-binding site that is lined by residues V69, F72, Y76, L131, L135, and I138 (Figure 2C), making the region very hydrophobic. The chemical property of this region is also preserved in eIF4E proteins from other organisms.²³ There is a small preformed pocket at the binding interface that acts as a docking site for the conserved leucine residue of the “YXXXXLΦ” motif present in the interacting eIF4G1 and 4E-BP1 peptides.^{14,15} In spite of the presence of this pocket, the binding region is almost planar, and in this state, the tryptophan adopts a conformation that is representative of the larger population ($\chi^2, 90\text{--}180^\circ$) sampled in the MD simulations and in the crystal structures (Figure 2A–C). However, during the simulations, when W73 adopts the conformation representative of the smaller populations ($\chi^2, 30^\circ\text{--}150^\circ$; combining range observed in holo and apo simulations), a new pocket that is cryptic in the other state emerges (Figure 2C,D) (movie S1). We term the conformation when W73 covers the cryptic pocket as the “closed state” and when the pocket is exposed as the “open state”. The cryptic pocket is also seen in solution-state structures of eIF4E in which W73 has flipped to the open state (Figure S2).

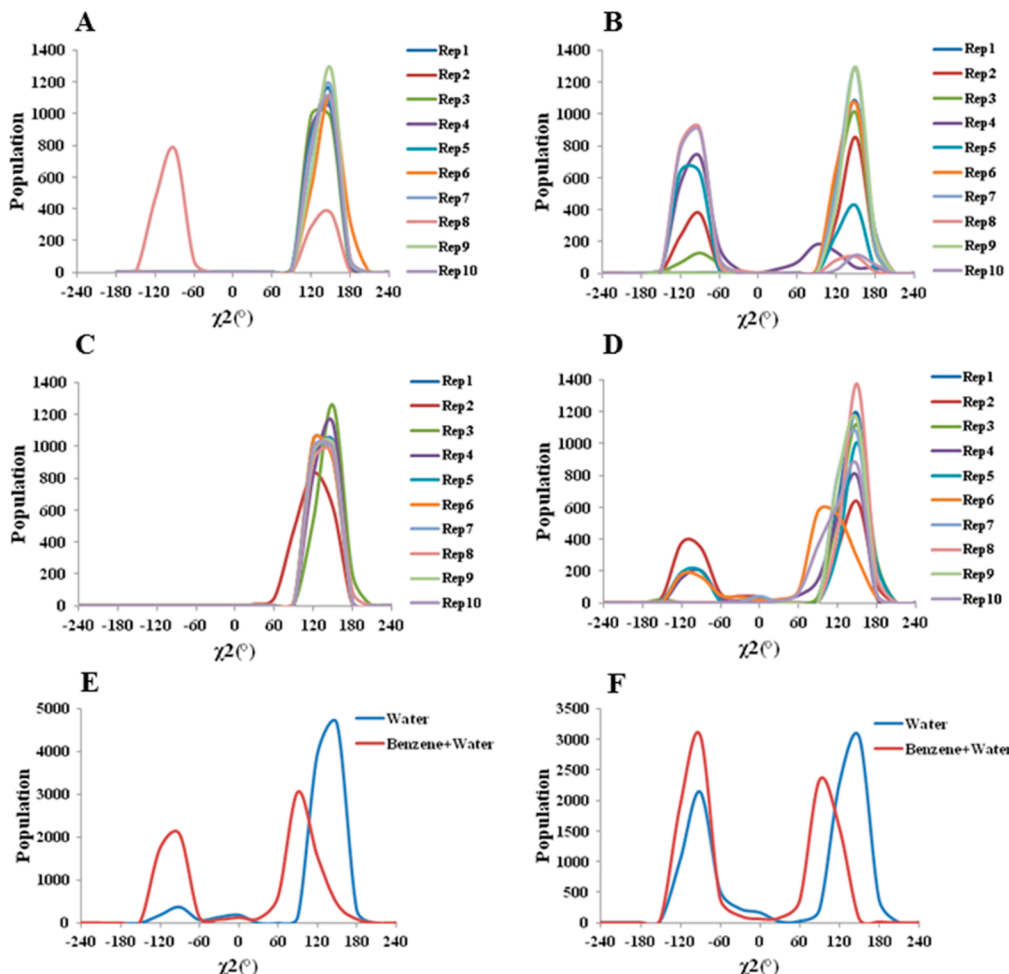


Figure 3. Population distribution of W73 between the open and closed states. The distribution was measured in terms of the χ^2 side-chain torsion angle in MD simulations of eIF4E under different simulation conditions. Ten replicates of 10 ns each starting from the (A and B) apo-state and (C and D) holo-state structure in pure water solvent and in 0.4 M benzene, respectively. (E and F) χ^2 distribution for a longer simulation period of 200 ns for the apo- and holo-state structures, respectively, of eIF4E in pure water and a 0.4 M mixture of benzene in water.

The creation of this pocket exposes hydrophobic regions that are energetically unfavorable in an aqueous environment, and this accounts for the transient nature of the open state (Figure 2B) in the MD simulations, and for its absence in the experimentally determined X-ray structures. In summary, it is clear that the open state conformation of W73 leads to the creation of a transiently exposed new cavity on the protein-binding interface of eIF4E.

Improved Accessibility of the Pocket in Mixed-Solvent Simulations. To further probe the transition of W73 and the associated opening of the underlying pocket, we conducted mixed-solvent MD simulations in which the biomolecule is simulated in a heterogeneous mixture of hydrophobic and hydrophilic solvents.^{37–41} This approach along with others has been used successfully to reveal cryptic potentially druggable pockets in proteins.^{37–41,57–61} Benzene was chosen as the hydrophobic solvent as it has recently been demonstrated to be a powerful probe^{39,40} for the identification of novel potential ligand-binding sites on proteins. An exhaustive set of all-atom MD simulations of eIF4E starting from pure water to mixed-solvent comprised of water and benzene were conducted (Table 2). The molar concentration of benzene was varied from 0.0 to 0.4 M in increments of 0.1 M. Concentrations above 0.4 M led to aggregation of benzene in the solution, indicating that the critical concentration for pronounced hydrophobic effects at this

volume had been reached. We set up 10 different starting states for each concentration in terms of the distribution of benzene molecules around the protein. A similar protocol was also followed for the pure water solvent following which a short 10 ns simulation was performed for each system. These simulations were separately conducted for the apo- and holo-states of the protein (Table 2), and in both starting structures, W73 was in the closed state.

In both the apo- and holo-protein simulations, it is observed that the open state becomes more accessible in the presence of benzene (Table 2 and Figure 3). In pure water, the open state is observed in only one instance during the time period of the simulations (Figure 3A,C). However, with the addition of benzene, a marked increase in the level of the open state is seen together with a gradual rise in the number of systems that sample this conformation (Table 2 and Figure 3B,D). At 0.4 M benzene, five trajectories of the holo and four of the apo simulations sample both states of W73. Thus, at this concentration, ~50% of the simulated cases show a tendency to explore both the conformational states as compared to almost none in the case of pure water. In addition to the improvement in sampling, the lifetime of the open state also increases (Figure S3A–D). This results from the stabilization of the open state in the presence of benzene molecules that occupy the exposed cavity. Along with

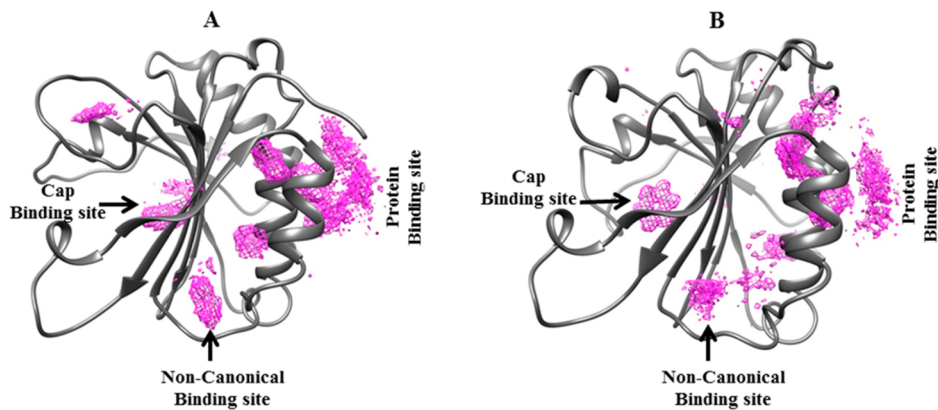


Figure 4. Multiple benzene-binding sites detected from mixed-solvent simulations. The benzene occupancy map is shown for the (A) apo-state and (B) holo-state structures of eIF4E. The map is displayed at an isovalue cutoff where there is no benzene cluster observed in the bulk. The protein- and cap-binding interfaces along with the noncanonical binding site are indicated.

the multiple short simulations, we also performed long simulations (200 ns each) for both the starting structures in pure solvent and at a benzene concentration of 0.4 M. W73 transiently samples both states in pure solvent as we had observed initially (Figure 3E,F and Figure S3E,F), although the holo structure exhibits sampling for the open state better than that of the apo structure. However, the residue remains mostly in the closed state. In contrast, in the hydrophobic medium, we see that W73 exists mostly in the open state (Figure 3E,F and Figure S3E,F). Thus, the mixed-solvent approach improves the transition of the residue to the alternate state, thereby increasing the accessibility of the pocket at the binding interface.

Binding of Benzene Molecules in the New Exposed Pocket. The benzene saturation simulations of eIF4E show multiple binding sites on the protein surface, which includes the canonical protein- and cap-binding interfaces (Figure 4). In addition, we also observe the presence of a benzene cluster at a site that was recently reported to be involved in the binding of noncanonical peptide motifs and a small molecule.^{62–65} It is very encouraging to see that our approach could indeed identify regions that are known binding interfaces and hence validates the method of identification of additional new binding sites on protein surfaces. We compared the conformational change of the hydrophobic residues present in the protein-binding interface between the crystal and simulated structures (Figure 5A,B). When the tryptophan residue is in the closed state, there is little change in conformation relative to other residues in the region. In the open state, the hydrophobic residues undergo a change in their conformations, especially residues V69, L135, and I138. This shows that the emergence of the cryptic pocket associated with the transition of W73 is also accompanied by a rearrangement of other residues in the binding interface. It is very interesting to observe that at the protein-binding interface, the water molecules are very dynamic as suggested by the lack of any substantial water cluster in this region (Figure 6A,C). In contrast, the benzene molecules seem to have a relatively higher residence time and hence appeared to be clustered at the interface (Figure 6B,D). The occupancy is appreciably high here compared to that of any other region in the protein. For both the starting structures, the randomly distributed benzenes in the solution (Figure S1) start crowding at this site during the simulations, suggesting that the region is preferentially solvated by the molecules of benzene. F72 is one of the deeply buried hydrophobic residues that gets exposed because of the transition

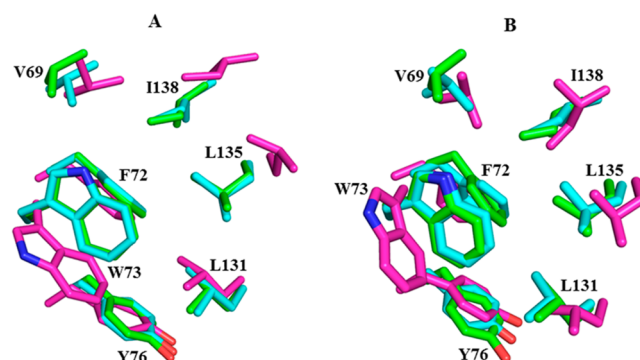


Figure 5. Superimposition of hydrophobic residues lining the protein-binding interface in eIF4E. The representation is shown for the (A) apo-state and (B) holo-state structures. In both cases, the crystal structure (green), the representative structure from the largest cluster (~49%) of the eIF4E simulation in pure water (cyan), and the representative structure from the largest cluster (~94%) from mixed water/benzene simulations (magenta) are shown. The representative structure from the simulation was obtained from the largest population derived by clustering the ensemble of structures based on the conformation of the hydrophobic residues.

of W73 and is present in the core of the newly formed pocket (Figure 5). We measured the number of benzene molecules that are present within 5 Å of the center of mass of F72 (Figure 7A). The maximal number of benzene molecules around the pocket was observed to be 6 in the case of the apo-state and 4 in the case of the holo-state simulations with the average value of ~3 (2.7 for apo and 2.8 for holo). Thus, the cryptic pocket is solvated by approximately three benzene molecules whose occupancy map is represented in panels B and C of Figure 7. The molecular surface of the protein depicting the shape of the pocket and the occupancy profile of the benzene molecules is different in both simulations. This reflects the plasticity and dynamic reorganization of the surrounding residues to accommodate the benzene molecules. In summary, we see that a highly plastic region of eIF4E is able to exist in states whereby a cryptic pocket transiently opens because of the flipping of W73, exposing a hydrophobic environment. The pocket can then be accessed and stabilized by other hydrophobic molecules such as benzene, thus suggesting it to be a potential binding site on eIF4E.

A Small Molecule Inhibitor Docks Favorably in the Newly Formed Cavity. A small molecule inhibitor (4E1RCat)

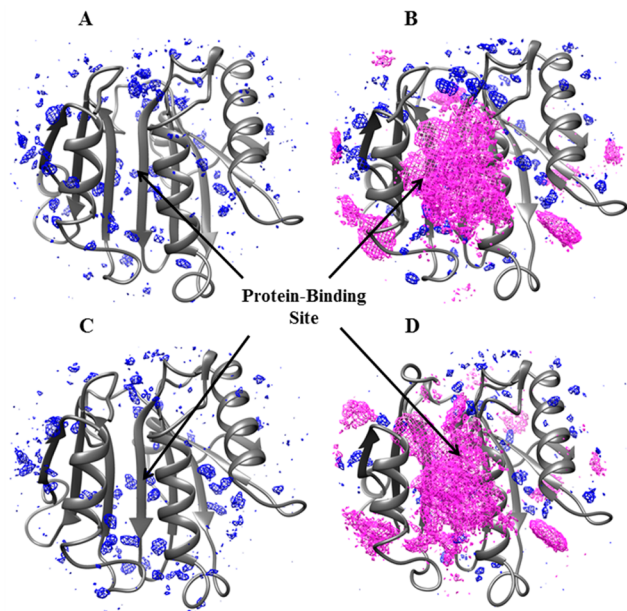


Figure 6. Occupancy map of water and benzene from mixed-solvent simulations. The map is shown for (A and C) water and (B and D) water and benzene in simulations of the apo- and holo-state structures of eIF4E, respectively, performed in pure solvent and 0.4 M benzene. The protein-binding site formed by helices H1 and H2 is represented with an arrow, and the largest difference in the occupancy profile is observed at this site.

of eIF4E that blocks its interactions with eIF4G1 and 4E-BP1 has been reported,¹⁰ which indicates that the molecule interacts at the protein-binding interface. A molecular model of this interaction has been suggested but with W73 in the closed state.¹⁰ We explored the possibility that the cryptic pocket observed in our current study would facilitate the interaction of this molecule at the interfacial region. Hence, we took two alternate states of the protein representing the open and closed states. The small molecule was then docked in both the states, and 20 different poses were generated (Figure 8A,B). It was interesting to observe that the ligand docked in multiple orientations around the binding interface in the case of the closed state conformation whereas we observe a very specific

binding mode for the open state. This difference is also reflected in the contrasting distribution of the docked population into different energy clusters for both states (Figure S4A,B). Interestingly, some of the docked poses in the closed state were similar to those modeled by Cenci et al.¹⁰ (Figure S4C), which reaffirms that it could be a preferred binding mode of the molecule in the absence of the cryptic pocket. However, in the open state complexes, the inhibitor binds in a distinct manner, and the benzene moiety present in the molecule explores the newly formed cavity because of the transition of W73 (Figure 8C).

We further compared the energetics of this complex by selecting three representative docked poses from the lowest-energy clusters (Figure S4A,B) of both the states and subjected them to 200 ns MD simulations each. The binding energy between the molecule and eIF4E was subsequently computed using the MM/GBSA methodology (Table 3). In all the calculations, the energy was found to be relatively more favorable when the small molecule interacts with eIF4E in the open state conformation. This study with the docking of the small molecule further substantiates our understanding that the newly formed cavity could be exploited for drug designing as it will likely facilitate a more favorable interaction of small molecules with eIF4E.

DISCUSSION

eIF4E is an important target for anticancer therapeutics, and the protein-binding interface between eIF4E and its binding partners is a prime focus for the design and development of inhibitors against the molecule. However, the protein-binding interface of eIF4E as revealed from structural studies appears to lack any distinct clefts and is largely flat, which makes the task of targeting this region for clinical applications challenging. Interestingly, our MD simulations of eIF4E reveal a rather dynamic landscape of the interfacial region, with a cryptic pocket appearing on the protein-binding surface. This pocket is revealed upon the conformational transition of an evolutionarily conserved tryptophan residue (W73). Solution-state structures of eIF4E^{54–56} had shown this residue in different possible conformations, including one that exposes the cryptic pocket, while the X-ray structures are characterized by a single conformational state^{25,28,51–53} wherein the pocket is occluded

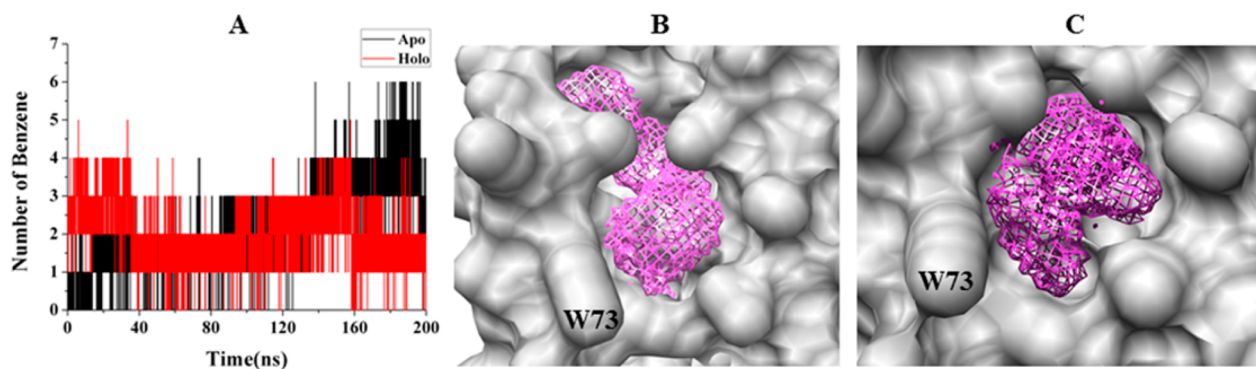


Figure 7. Number of benzene molecules and occupancy map of benzene around the exposed pocket. (A) The number of benzene molecules was calculated around F72, which is one of the hydrophobic residues exposed (see Figure 5) during the transition of W73. The average number of benzene molecules in both the apo and holo structures is calculated to be \sim 3 (2.7 for apo and 2.8 for holo). (B and C) The occupancy map of three benzene molecules is represented for both the apo- and holo-state simulations, respectively. The average structure for both the simulations is shown, and the exposed cavity accommodates the three benzene molecules by modulating its binding interface, which signifies the ligandibility and plasticity of this new pocket.

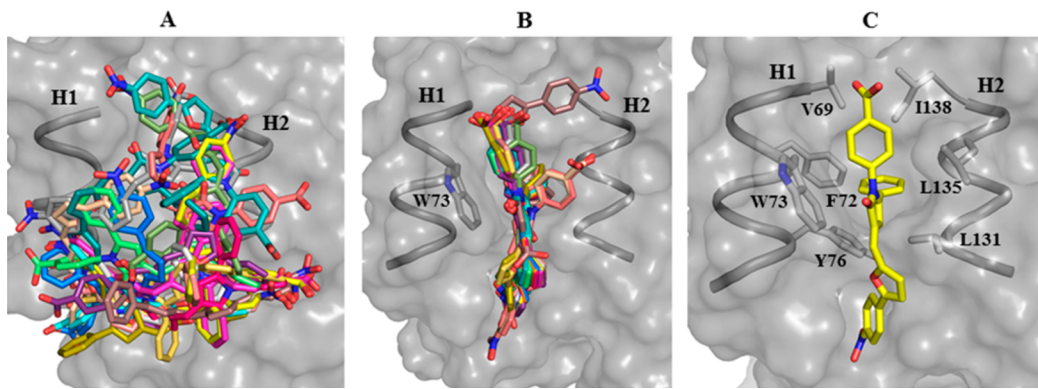


Figure 8. Docking of small molecule 4E1RCat with eIF4E. The twenty lowest-energy docked poses are shown each for the (A) closed and (B) open states. The molecule has multiple docked orientations in the closed structure, whereas it displays a specific docking orientation in the open state structure. (C) Representative structure from the open state docked complex indicating the occupancy of the cryptic pocket by the benzene moiety of the small molecule.

Table 3. Computed Binding Energies of the Small Molecule Ligand 4E1RCat with eIF4E^a

complex	closed state (kcal/mol)	open state (kcal/mol)
Pose_1	-19.3 ± 3.4	-24.8 ± 2.8
Pose_2	-21.0 ± 3.4	-29.9 ± 5.0
Pose_3	-20.0 ± 3.5	-28.8 ± 3.6

^aThe binding energy was calculated using MM/GBSA as described in Materials and Methods. The representative starting state (Pose_1, Pose_2, and Pose_3) of the protein–ligand complex for MD simulations was selected from the first three lowest-energy clusters of the docked complexes in both states (see Figure S4A,B).

from solvent. In contrast, MD simulations starting from the X-ray-determined structures capture W73 in different states encompassing those observed in the representative experimental structures of the protein in solution. The opening of the cryptic pocket exposes a pronounced hydrophobic cavity that appears to be amenable for the binding of hydrophobic molecules. The pocket becomes more accessible in a relatively hydrophobic medium (benzene molecules dispersed in water were used in this study), which suggests that an external factor could be used to influence the triggering of the pocket to open. A similar approach using SILCS (site identification by ligand competitive saturation) with hydrophobic fragments was able to induce the recognition of two well-characterized cryptic pockets in cytokine interleukin-2 that are otherwise occluded in the unbound state of the protein.⁵⁷ The benzene saturation simulation as used in this study has been successfully applied to design a specific ligand that targets a cryptic binding pocket on the surface of Polo-like kinase 1 protein.⁴⁰

Small molecules have been reported to interact with eIF4E potentially at the protein-binding interface.^{10,13} Docking and simulation of one such compound, 4E1RCat, onto eIF4E in the absence and presence of the exposed cryptic binding site indicate that the molecule interacts more favorably with the latter. This suggests that the cryptic pocket could provide an alternate binding mechanism for the molecules. This observation becomes more significant in light of the recent development in which a noncanonical binding interface has been detected in eIF4E, which binds both small molecule and peptide motifs.^{62–65} This interface was also observed to bind clusters of benzene in our simulation (Figure 4). The dynamic and plastic nature of the protein-binding interface in eIF4E is also highlighted by the fact that the RING domain of arenaviral protein Z from Lassa fever

virus is reported to bind eIF4E in a mode that is distinct from the canonical binding mode of other eIF4E-interacting peptides.²⁷ Interestingly, in their study, the authors also observe that W73 undergoes the largest chemical shift during the interaction of the RING domain with the protein. Taken together, our study has identified a cryptic hydrophobic pocket on the protein-binding interface of eIF4E whose exposure is controlled through gating by a conserved tryptophan residue. Small molecules could favorably be accommodated in this cavity, which indicates that the newly formed cleft could act as a novel interacting site with potential therapeutic applications. These observations make for a compelling argument in favor of the exploitation of this new pocket for the development of new lead inhibitor molecules against the oncogenic eIF4E protein.

ASSOCIATED CONTENT

Supporting Information

The Supporting Information is available free of charge on the ACS Publications website at DOI: 10.1021/acs.biochem.5b00812.

Illustrative example of eIF4E protein solvated in water and benzene for mixed-solvent simulations (Figure S1), representative examples from NMR-resolved structures of eIF4E that show the different conformational states of W73 in solution and the presence of the cryptic pocket (Figure S2), time series plot of the side-chain χ^2 torsion angle of tryptophan 73 in pure water and in a mixture with benzene (Figure S3), energy-based clustering plot of docked structures of the small molecule 4E1RCat with eIF4E and a representative example from the open state docked complex (Figure S4), and a simulation movie of eIF4E depicting the transition of tryptophan 73 and exposure of the cryptic pocket (Movie S1) (PDF)

AUTHOR INFORMATION

Corresponding Authors

*Bioinformatics Institute, A*STAR (Agency for Science, Technology and Research), 30 Biopolis St., #07-01 Matrix, Singapore 138671. E-mail: dilrajl@bii.a-star.edu.sg. Telephone: (65) 6478 8499. Fax: (65) 6478 9047.

*Bioinformatics Institute, A*STAR (Agency for Science, Technology and Research), 30 Biopolis St., #07-01 Matrix, Singapore 138671. E-mail: chandra@bii.a-star.edu.sg. Telephone: (65) 6478 8273. Fax: (65) 6478 9048.

Notes

The authors declare no competing financial interest.

ACKNOWLEDGMENTS

We thank Dr. Tan Yaw Sing for assisting in setting up the mixed-solvent simulations and Dr. Garima Tiwari for guidance in using the AutoDock program. We also thank all the members of the group for helpful discussions and suggestions.

ABBREVIATIONS

eiF, eukaryotic initiation factor; 4E-BP, 4E-binding protein; PDB, Protein Data Bank; NMR, nuclear magnetic resonance; AMBER, Assisted Model Building with Energy Refinement; PMEMD, Particle Mesh Ewald Molecular Dynamics; GAFF, Generalized Amber Force Field.

REFERENCES

- (1) Jia, Y., Polunovsky, V., Bitterman, P. B., and Wagner, C. R. (2012) Cap-dependent translation initiation factor eIF4E: an emerging anticancer drug target. *Med. Res. Rev.* 32, 786–814.
- (2) Rhoads, R. E. (2009) eIF4E: new family members, new binding partners, new roles. *J. Biol. Chem.* 284, 16711–16715.
- (3) Carroll, M., and Borden, K. L. (2013) The oncogene eIF4E: using biochemical insights to target cancer. *J. Interferon Cytokine Res.* 33, 227–238.
- (4) Dua, K., Williams, T. M., and Beretta, L. (2001) Translational control of the proteome: relevance to cancer. *Proteomics* 1, 1191–1199.
- (5) Mamane, Y., Petroulakis, E., Rong, L., Yoshida, K., Ler, L. W., and Sonenberg, N. (2004) eIF4E—from translation to transformation. *Oncogene* 23, 3172–3179.
- (6) Borden, K. L. (2011) Targeting the oncogene eIF4E in cancer: From the bench to clinical trials. *Clin. Invest. Med.* 34, E315.
- (7) Hsieh, A. C., and Ruggiero, D. (2010) Targeting eukaryotic translation initiation factor 4E (eIF4E) in cancer. *Clin. Cancer Res.* 16, 4914–4920.
- (8) Bhattacharyya, D., Nguyen, K., and Basu, S. (2014) Rationally induced RNA:DNA G-quadruplex structures elicit an anticancer effect by inhibiting endogenous eIF-4E expression. *Biochemistry* 53, 5461–5470.
- (9) Brown, C. J., Lim, J. J., Leonard, T., Lim, H. C., Chia, C. S., Verma, C. S., and Lane, D. P. (2011) Stabilizing the eIF4G1 alpha-helix increases its binding affinity with eIF4E: implications for peptidomimetic design strategies. *J. Mol. Biol.* 405, 736–753.
- (10) Cencic, R., Hall, D. R., Robert, F., Du, Y., Min, J., Li, L., Qui, M., Lewis, I., Kurtkaya, S., Dingledine, R., Fu, H., Kozakov, D., Vajda, S., and Pelletier, J. (2011) Reversing chemoresistance by small molecule inhibition of the translation initiation complex eIF4F. *Proc. Natl. Acad. Sci. U. S. A.* 108, 1046–1051.
- (11) Chen, X., Kopecky, D. J., Mihalic, J., Jeffries, S., Min, X., Heath, J., Deignan, J., Lai, S., Fu, Z., Guimaraes, C., Shen, S., Li, S., Johnstone, S., Thibault, S., Xu, H., Cardozo, M., Shen, W., Walker, N., Kayser, F., and Wang, Z. (2012) Structure-guided design, synthesis, and evaluation of guanine-derived inhibitors of the eIF4E mRNA-cap interaction. *J. Med. Chem.* 55, 3837–3851.
- (12) Lama, D., Quah, S. T., Verma, C. S., Lakshminarayanan, R., Beuerman, R. W., Lane, D. P., and Brown, C. J. (2013) Rational optimization of conformational effects induced by hydrocarbon staples in peptides and their binding interfaces. *Sci. Rep.* 3, 3451.
- (13) Moerke, N. J., Aktas, H., Chen, H., Cantel, S., Reibarkh, M. Y., Fahmy, A., Gross, J. D., Degterev, A., Yuan, J., Chorev, M., Halperin, J. A., and Wagner, G. (2007) Small-molecule inhibition of the interaction between the translation initiation factors eIF4E and eIF4G. *Cell* 128, 257–267.
- (14) Brown, C. J., McNae, I., Fischer, P. M., and Walkinshaw, M. D. (2007) Crystallographic and mass spectrometric characterisation of eIF4E with N7-alkylated cap derivatives. *J. Mol. Biol.* 372, 7–15.
- (15) Brown, C. J., Verma, C. S., Walkinshaw, M. D., and Lane, D. P. (2009) Crystallization of eIF4E complexed with eIF4G1 peptide and glycerol reveals distinct structural differences around the cap-binding site. *Cell Cycle* 8, 1905–1911.
- (16) Martineau, Y., Azar, R., Bousquet, C., and Pyronnet, S. (2013) Anti-oncogenic potential of the eIF4E-binding proteins. *Oncogene* 32, 671–677.
- (17) Zhou, W., Quah, S. T., Verma, C. S., Liu, Y., Lane, D. P., and Brown, C. J. (2012) Improved eIF4E binding peptides by phage display guided design: plasticity of interacting surfaces yield collective effects. *PLoS One* 7, e47235.
- (18) Kussie, P. H., Gorina, S., Marechal, V., Elenbaas, B., Moreau, J., Levine, A. J., and Pavletich, N. P. (1996) Structure of the MDM2 oncoprotein bound to the p53 tumor suppressor transactivation domain. *Science* 274, 948–953.
- (19) Lama, D., Modi, V., and Sankararamakrishnan, R. (2013) Behavior of solvent-exposed hydrophobic groove in the anti-apoptotic Bcl-XL protein: clues for its ability to bind diverse BH3 ligands from MD simulations. *PLoS One* 8, e54397.
- (20) Lama, D., and Sankararamakrishnan, R. (2010) Identification of core structural residues in the sequentially diverse and structurally homologous Bcl-2 family of proteins. *Biochemistry* 49, 2574–2584.
- (21) Assouline, S., Culjkovic, B., Cocolakis, E., Rousseau, C., Beslu, N., Amri, A., Caplan, S., Leber, B., Roy, D. C., Miller, W. H., Jr., and Borden, K. L. (2009) Molecular targeting of the oncogene eIF4E in acute myeloid leukemia (AML): a proof-of-principle clinical trial with ribavirin. *Blood* 114, 257–260.
- (22) Kentsis, A., Topisirovic, I., Culjkovic, B., Shao, L., and Borden, K. L. (2004) Ribavirin suppresses eIF4E-mediated oncogenic transformation by physical mimicry of the 7-methyl guanosine mRNA cap. *Proc. Natl. Acad. Sci. U. S. A.* 101, 18105–18110.
- (23) Joshi, B., Lee, K., Maeder, D. L., and Jagus, R. (2005) Phylogenetic analysis of eIF4E-family members. *BMC Evol. Biol.* 5, 48.
- (24) Mader, S., Lee, H., Pause, A., and Sonenberg, N. (1995) The translation initiation factor eIF-4 gamma and the translational repressors 4E-binding proteins. *Mol. Cell. Biol.* 15, 4990–4997.
- (25) Marcotrigiano, J., Gingras, A. C., Sonenberg, N., and Burley, S. K. (1997) Cocrystal structure of the messenger RNA 5' cap-binding protein (eIF4E) bound to 7-methyl-GDP. *Cell* 89, 951–961.
- (26) Kentsis, A., Dwyer, E. C., Perez, J. M., Sharma, M., Chen, A., Pan, Z. Q., and Borden, K. L. (2001) The RING domains of the promyelocytic leukemia protein PML and the arenaviral protein Z repress translation by directly inhibiting translation initiation factor eIF4E. *J. Mol. Biol.* 312, 609–623.
- (27) Volpon, L., Osborne, M. J., Capul, A. A., de la Torre, J. C., and Borden, K. L. (2010) Structural characterization of the Z RING-eIF4E complex reveals a distinct mode of control for eIF4E. *Proc. Natl. Acad. Sci. U. S. A.* 107, 5441–5446.
- (28) Siddiqui, N., Tempel, W., Nediyalkova, L., Volpon, L., Wernimont, A. K., Osborne, M. J., Park, H. W., and Borden, K. L. (2012) Structural insights into the allosteric effects of 4EBP1 on the eukaryotic translation initiation factor eIF4E. *J. Mol. Biol.* 415, 781–792.
- (29) Jorgensen, W. L., Chandrasekhar, J., Madura, J. D., Impey, W. R., and Klein, M. L. (1983) Comparison of simple potential functions for simulating liquid water. *J. Chem. Phys.* 79, 926–935.
- (30) Case, D. A., Darden, T. A., Cheatham, T. E., III, Simmerling, C. L., Wang, J., Duke, R. E., Luo, R., Walker, R. C., Zhang, W., Merz, K. M., Roberts, B., Hayik, S., Roitberg, A., Seabra, G., Swails, J., Gotz, A. W., Kolossvary, I., Wong, K. F., Paesani, F., Vanicek, J., Wolf, R. M., Liu, J., Wu, X., Brozell, S. R., Steinbrecher, T., Gohlke, H., Cai, Q., Ye, X., Wang, J., Hsieh, M.-J., Cui, G., Roe, D. R., Mathews, D. H., Seetin, M. G., Salomon-Ferrer, R., Sagui, C., Babin, V., Luchko, S., Gusalov, S., Kovalenko, A., and Kollman, P. A. (2012) AMBER 12, University of California, San Francisco.
- (31) Hornak, V., Abel, R., Okur, A., Strockbine, B., Roitberg, A., and Simmerling, C. (2006) Comparison of multiple Amber force fields and development of improved protein backbone parameters. *Proteins: Struct., Funct., Genet.* 65, 712–725.

- (32) Loncharich, R. J., Brooks, B. R., and Pastor, R. W. (1992) Langevin dynamics of peptides: the frictional dependence of isomerization rates of N-acetylalanyl-N'-methylamide. *Biopolymers* 32, 523–535.
- (33) Pastor, R. W., Brooks, B. R., and Szabo, A. (1988) An analysis of the accuracy of Langevin and molecular dynamics algorithms. *Mol. Phys.* 65, 1409–1419.
- (34) Berendsen, H. J. C., Postma, J. P. M., Van Gunsteren, W. F., DiNola, A., and Haak, J. R. (1984) Molecular Dynamics with coupling to an external bath. *J. Chem. Phys.* 81, 3684–3690.
- (35) Darden, T., York, D., and Pedersen, L. (1993) Particle mesh Ewald-an Nlog(N) method for Ewald sums in large systems. *J. Chem. Phys.* 98, 10089–10092.
- (36) Ryckaert, J.-P., Ciccotti, G., and Berendsen, H. J. C. (1977) Numerical Integration of the cartesian equations of motion of a system with constraints: Molecular dynamics of n-alkanes. *J. Comput. Phys.* 23, 327–341.
- (37) Yang, C.-Y., and Wang, S. (2011) Hydrophobic Binding Hot Spots of Bcl-XL Protein-Protein Interfaces by Cosolvent Molecular Dynamics Simulation. *ACS Med. Chem. Lett.* 2, 280–284.
- (38) Lexa, K. W., and Carlson, H. A. (2013) Improving protocols for protein mapping through proper comparison to crystallography data. *J. Chem. Inf. Model.* 53, 391–402.
- (39) Tan, Y. S., Spring, D. R., Abell, C., and Verma, C. S. (2015) The Application of Ligand-Mapping Molecular Dynamics Simulations to the Rational Design of Peptidic Modulators of Protein-Protein Interactions. *J. Chem. Theory Comput.* 11, 3199–3210.
- (40) Tan, Y. S., Sledz, P., Lang, S., Stubbs, C. J., Spring, D. R., Abell, C., and Best, R. B. (2012) Using ligand-mapping simulations to design a ligand selectively targeting a cryptic surface pocket of polo-like kinase 1. *Angew. Chem., Int. Ed.* 51, 10078–10081.
- (41) Tan, Y. S., Spring, D. R., Abell, C., and Verma, C. S. (2014) The Use of Chlorobenzene as a Probe Molecule in Molecular Dynamics Simulations. *J. Chem. Inf. Model.* 54, 1821–1827.
- (42) Martinez, L., Andrade, R., Birgin, E. G., and Martinez, J. M. (2009) PACKMOL: a package for building initial configurations for molecular dynamics simulations. *J. Comput. Chem.* 30, 2157–2164.
- (43) Dupradeau, F. Y., Cezard, C., Lelong, R., Stanislawaik, E., Pecher, J., Delepine, J. C., and Cieplak, P. (2007) R.E.D.D.B.: a database for RESP and ESP atomic charges, and force field libraries. *Nucleic Acids Res.* 36, D360–D367.
- (44) Wang, J., Wolf, R. M., Caldwell, J. W., Kollman, P. A., and Case, D. A. (2004) Development and testing of a general amber force field. *J. Comput. Chem.* 25, 1157–1174.
- (45) Pettersen, E. F., Goddard, T. D., Huang, C. C., Couch, G. S., Greenblatt, D. M., Meng, E. C., and Ferrin, T. E. (2004) UCSF Chimera—a visualization system for exploratory research and analysis. *J. Comput. Chem.* 25, 1605–1612.
- (46) Morris, G. M., Huey, R., Lindstrom, W., Sanner, M. F., Belew, R. K., Goodsell, D. S., and Olson, A. J. (2009) AutoDock4 and AutoDockTools4: Automated docking with selective receptor flexibility. *J. Comput. Chem.* 30, 2785–2791.
- (47) Vanquelef, E., Simon, S., Marquant, G., Garcia, E., Klimerak, G., Delepine, J. C., Cieplak, P., and Dupradeau, F. Y. (2011) R.E.D. Server: a web service for deriving RESP and ESP charges and building force field libraries for new molecules and molecular fragments. *Nucleic Acids Res.* 39, W511–517.
- (48) Bashford, D., and Case, D. A. (2000) Generalized born models of macromolecular solvation effects. *Annu. Rev. Phys. Chem.* 51, 129–152.
- (49) Miller, B. R. I., McGee, D. T. J., Swails, J. M., Homeyer, N., Gohlke, H., and Roitberg, A. E. (2012) MMPBSA.py: An Efficient Program for End-State Energy Calculations. *J. Chem. Theory Comput.* 8, 3314–3321.
- (50) Onufriev, A., Bashford, D., and Case, D. A. (2004) Exploring protein native states and large-scale conformational changes with a modified generalized born model. *Proteins: Struct., Funct., Genet.* 55, 383–394.
- (51) Ashby, J. A., Stevenson, C. E., Jarvis, G. E., Lawson, D. M., and Maule, A. J. (2011) Structure-based mutational analysis of eIF4E in relation to sbm1 resistance to pea seed-borne mosaic virus in pea. *PLoS One* 6, e15873.
- (52) Monzingo, A. F., Dhaliwal, S., Dutt-Chaudhuri, A., Lyon, A., Sadow, J. H., Hoffman, D. W., Robertus, J. D., and Browning, K. S. (2007) The structure of eukaryotic translation initiation factor-4E from wheat reveals a novel disulfide bond. *Plant Physiol.* 143, 1504–1518.
- (53) Niedzwiecka, A., Marcotrigiano, J., Stepinski, J., Jankowska-Anyszka, M., Wyslouch-Cieszynska, A., Dadlez, M., Gingras, A. C., Mak, P., Darzynkiewicz, E., Sonenberg, N., Burley, S. K., and Stolarski, R. (2002) Biophysical studies of eIF4E cap-binding protein: recognition of mRNA 5' cap structure and synthetic fragments of eIF4G and 4E-BP1 proteins. *J. Mol. Biol.* 319, 615–635.
- (54) Gross, J. D., Moerke, N. J., von der Haar, T., Lugovskoy, A. A., Sachs, A. B., McCarthy, J. E., and Wagner, G. (2003) Ribosome loading onto the mRNA cap is driven by conformational coupling between eIF4G and eIF4E. *Cell* 115, 739–750.
- (55) Matsuo, H., Li, H., McGuire, A. M., Fletcher, C. M., Gingras, A. C., Sonenberg, N., and Wagner, G. (1997) Structure of translation factor eIF4E bound to m7GDP and interaction with 4E-binding protein. *Nat. Struct. Biol.* 4, 717–724.
- (56) Volpon, L., Osborne, M. J., Topisirovic, I., Siddiqui, N., and Borden, K. L. (2006) Cap-free structure of eIF4E suggests a basis for conformational regulation by its ligands. *EMBO J.* 25, 5138–5149.
- (57) Foster, T. J., MacKerell, A. D., Jr., and Guvench, O. (2012) Balancing target flexibility and target denaturation in computational fragment-based inhibitor discovery. *J. Comput. Chem.* 33, 1880–1891.
- (58) Guvench, O., and MacKerell, A. D., Jr. (2009) Computational fragment-based binding site identification by ligand competitive saturation. *PLoS Comput. Biol.* 5, e1000435.
- (59) Lexa, K. W., and Carlson, H. A. (2011) Full protein flexibility is essential for proper hot-spot mapping. *J. Am. Chem. Soc.* 133, 200–202.
- (60) Raman, E. P., Yu, W., Guvench, O., and Mackerell, A. D. (2011) Reproducing crystal binding modes of ligand functional groups using Site-Identification by Ligand Competitive Saturation (SILCS) simulations. *J. Chem. Inf. Model.* 51, 877–896.
- (61) Johnson, D. K., and Karanicolas, J. (2013) Druggable protein interaction sites are more predisposed to surface pocket formation than the rest of the protein surface. *PLoS Comput. Biol.* 9, e1002951.
- (62) Kinkelin, K., Veith, K., Grunwald, M., and Bono, F. (2012) Crystal structure of a minimal eIF4E-Cup complex reveals a general mechanism of eIF4E regulation in translational repression. *RNA* 18, 1624–1634.
- (63) Papadopoulos, E., Jenni, S., Kabha, E., Takrouri, K. J., Yi, T., Salvi, N., Luna, R. E., Gavathiotis, E., Mahalingam, P., Arthanari, H., Rodriguez-Mias, R., Yefidoff-Freedman, R., Aktas, B. H., Chorev, M., Halperin, J. A., and Wagner, G. (2014) Structure of the eukaryotic translation initiation factor eIF4E in complex with 4EGI-1 reveals an allosteric mechanism for dissociating eIF4G. *Proc. Natl. Acad. Sci. U. S. A.* 111, E3187–3195.
- (64) Peter, D., Igrelja, C., Weber, R., Wohlbolt, L., Weiler, C., Ebertsch, L., Weichenrieder, O., and Izaurralde, E. (2015) Molecular architecture of 4E-BP translational inhibitors bound to eIF4E. *Mol. Cell* 57, 1074–1087.
- (65) Sekiyama, N., Arthanari, H., Papadopoulos, E., Rodriguez-Mias, R. A., Wagner, G., and Leger-Abraham, M. (2015) Molecular mechanism of the dual activity of 4EGI-1: Dissociating eIF4G from eIF4E but stabilizing the binding of unphosphorylated 4E-BP1. *Proc. Natl. Acad. Sci. U. S. A.* 112, E4036–4045.